New (Iso)Quinolinyl-Pyridine-2,6-dicarboxamide G-Quadruplex ligands. A Structure-Activity Relationship Study

Enrico Cadoni [1], Pedro R. Magalhães [2], Rita Emídio [2], Eduarda Mendes [1,3], Jorge B. Vítor [4], Josué Carvalho [5], Carla Cruz [5], Bruno L. Victor [2] and Alexandra Paulo [1,3,*]

[1] Research Institute for Medicines (iMed.ULisboa), Faculty of Pharmacy, Universidade de Lisboa, Av. Prof. Gama Pinto, 1649-003 Lisboa, Portugal;

[2] BioISI - Biosystems & Integrative Sciences Institute, Faculty of Sciences, University of Lisboa, Campo Grande, C8 bdg, 1749-016 Lisboa, Portugal

[3] Dep. of Pharmaceutical Sciences and Medicines, Faculty of Pharmacy, Universidade de Lisboa, Av. Prof. Gama Pinto, 1649-003 Lisboa, Portugal;

[4] Dep. of Pharmacy, Pharmacology and Health Technologies, Faculty of Pharmacy, Universidade de Lisboa, Av. Prof. Gama Pinto, 1649-003 Lisboa, Portugal;

[5] CICS-UBI - Centro de Investigação em Ciências da Saúde, Universidade da Beira Interior, Av. Infante D. Henrique, 6200-506, Covilhã, Portugal

*Correspondence: mapaulo@ff.ulisboa.pt;

Supplementary Materials

1. General

All the reagents were purchased from Sigma-Aldrich and Merck and used without further purification.

NMR-Spectra were recorded on a Bruker 300 Ultrashield 300MHz, using 300 MHz scan for 1H-NMR spectra and 75 MHz for 13C.

Purity of compounds submitted to biophysical, biochemical or biological tests were in all cases > 90 % as determined by HPLC–DAD-MS (HPLC Waters Alliance 2695 coupled to a Photodiode Array Detector Waters 996 PDA and a Triple Quadrupole MS Micromass Quattro Micro API)

2. FRET melting experiments

FRET melting assays were performed on a 7300 RT-PCR equipment from Applied Biosystems. The test compound solutions (50 µL) were distributed across 96-well RT-PCR plates (PCR-96-FLT-C, Axygen, Inc.).

Standard and labelled HPLC-purified oligonucleotides were purchased from STABVIDA (Portugal), and sequences are depicted in table **S1**.

Table S1. Sequences used in FRET-melting experiments.

Name	**Sequence**	**Topology**	**Tm (°C)**
k-RAS	5'-FAM-AGGGCGGTGTGGGAAGAGGGA-TAMRA-3'	Parallel G4	49.0 ± 0.2
h-Telo	5'-FAM-GGGTTAGGGTTAGGGTTAGGG-TAMRA-3'	Hybrid G4	56.9 ± 0.2
T-Loop	5'-FAM-TATAGCTATATTTTTTTATAGCTATA-TAMRA-3'	dsDNA	53.2 ± 1.0
26merA	5'-CAATCGGATCGAATTCGATCCGATTG-3'	ssDNA	
26merB	5'-GTTAGCCTAGCTTAAGCTAGGCTAAG-3'	ssDNA	

3. CD Titrations

CD titrations and melting assays were performed on Jasco J-815 spectrapolarimeter equipped with a Peltier-type temperature control system (model CDF-426S/15), using an instrument scanning speed of 200 nm/min with a response time of 1 s in wavelengths ranging from 200 to 340 nm. The DNA sequences used for the experiments, and their respective melting temperatures are depicted in table S2.

Table S2. Sequences used in CD experiments.

Name	**Sequence**	**Topology**	**Tm (°C)**
k-RAS	5'-AGGGCGGTGTGGGAAGAGGGA- 3'	Parallel G4	48.3 ± 0.2
H-Telo	5'- GGGTTAGGGTTAGGGTTAGGG-3'	Hybrid G4	59.6 ± 0.9
c-MYC	5'-TGGGGAGGGTGGGGAGGGT- 3'	Parallel G4	50.4 ± 1.9

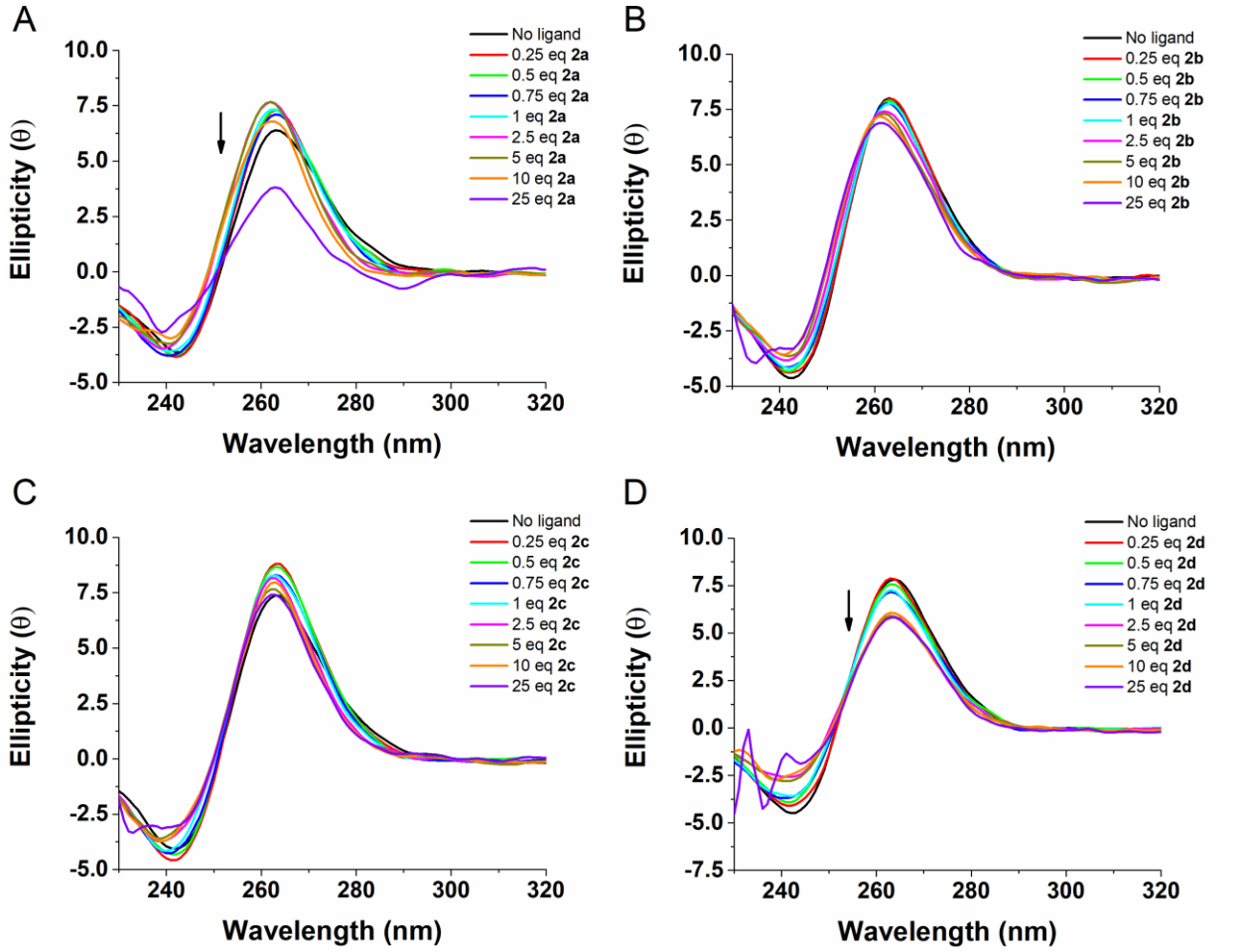

Figure S1. CD titration of c-MYC in presence of increasing equivalents (0-25) of compound 2a (A), 2b (B), 2c (C), 2d (D), at a concentration of 10 µM, performed in 20 mM lithium cacodylate containing 100 mM LiCl.

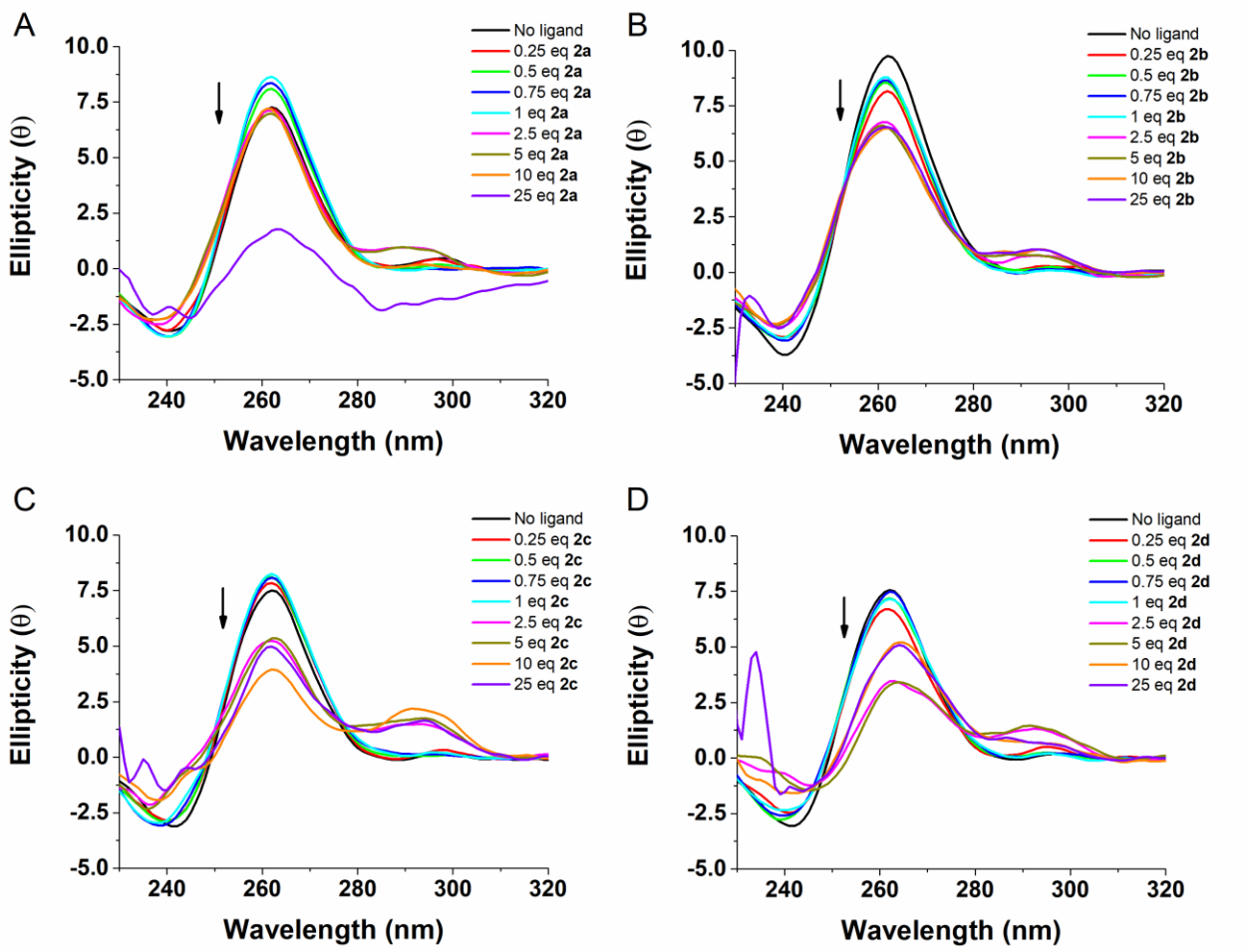

Figure S2. CD titration of k-RAS in presence of increasing equivalents (0-25) of compound 2a (A), 2b (B), 2c (C), 2d (D), at a concentration of 10 µM, performed in 20 mM lithium cacodylate containing 50 mM KCl for k-RAS.

4. PCR-Stop assay

The primer sequences used in PCR-stop assay are depicted in table S3. Sequence-design was adapted from [1].

Table S3. Sequences used in PCR-stop assay

Name	**Sequence**
Pu27	5'-TGGGGAGGGTGGGGAGGGTGGGGAAGG-3'
Pu27mut	5'-TGGGGAGGGTGGAAAGGGTGGGGAAGG-3'
Pu27REV	5'-ATCGAATCGCTTCTCGTCCTTCCCCA-3'

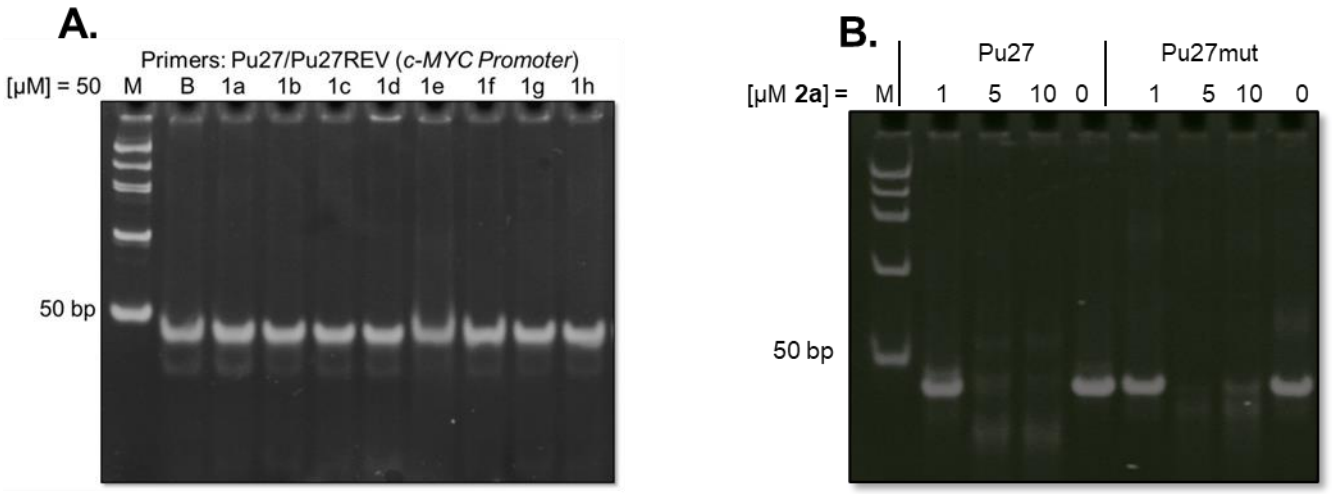

*Figure S3. A) Results of PCR-stop assay of compounds **1a-h** at 50 µM with c-MYC gene promoter Pu27. B) Results of PCR-stop assay of compound **2a** with c-MYC gene promoter Pu27 and with mutated c-MYC gene promoter (Pu27mut). In absence of compound, the 43 bp PCR products from constructions with Pu27 is formed.*

5. MM/PBSA calculations

The equation used to determine the binding free energy of the ligands to the quadruplex is expressed as:

$$\Delta G_{bind} = \Delta G_{complex}^{vdW} + \Delta G_{complex}^{ele} + \Delta G^{polar} + \Delta G^{nonpolar} \quad \text{(eq 1)}$$

with $V_{complex}$vdW and $V_{complex}$ele being the quadruplex–ligand van der Waals and electrostatic interaction energies, respectively. The polar and the nonpolar contributions are expressed as

$$\Delta G^{polar} = G_{complex}^{polar} - (G_{protein}^{polar} + G_{ligand}^{polar}) \quad \text{(eq 2)}$$

and

$$\Delta G^{nonpolar} = G_{complex}^{nonpolar} - (G_{protein}^{nonpolar} + G_{ligand}^{nonpolar}) \quad \text{(eq 3)}$$

The Poisson–Boltzmann (PB) equation for the polar term is evaluated using the following equation:

$$\nabla \cdot [\varepsilon(r)\nabla \cdot \varphi(r)] - \varepsilon(r)k(r)^2 \sinh[\varphi(r)] + \frac{4\pi\rho^f(r)}{k_B T} = 0 \quad \text{(eq 4)}$$

where ϕ(r) corresponds to the ligand's electrostatic potential, ε(r) the dielectric constant, and $\rho^f(r)$ the fixed charge density. Since the polar solvation energy is known to depend on the chosen value for the dielectric constant ε_{solute} of the complex [2], several values (2, 4 and 8) were evaluated to inspect its effect on predicted ΔG_{bind} values. By default, ε_{solute} is set to 2, but ultimately, we have used a value of 8 which showed to be the most adequate to use for our system. All the other settings in g_mmpbsa were left unaltered (i.e., use of atomic radii as proposed by Bondi [3], linear PB equation solver, 0.05 nm grid resolution, and smoothed van der Waals surface).

To estimate nonpolar solvation energies, we have used a linear dependence of $G_{nonpolar}$ on the SASA, expressed as follows [4]:

$$G^{nonpolar} = \gamma_{surf} SASA + b \quad \text{(eq 5)}$$

where γ_{surf} is related to the surface tension of the solvent. A solvent probe radius of 0.14 nm was used to determine the SASA.

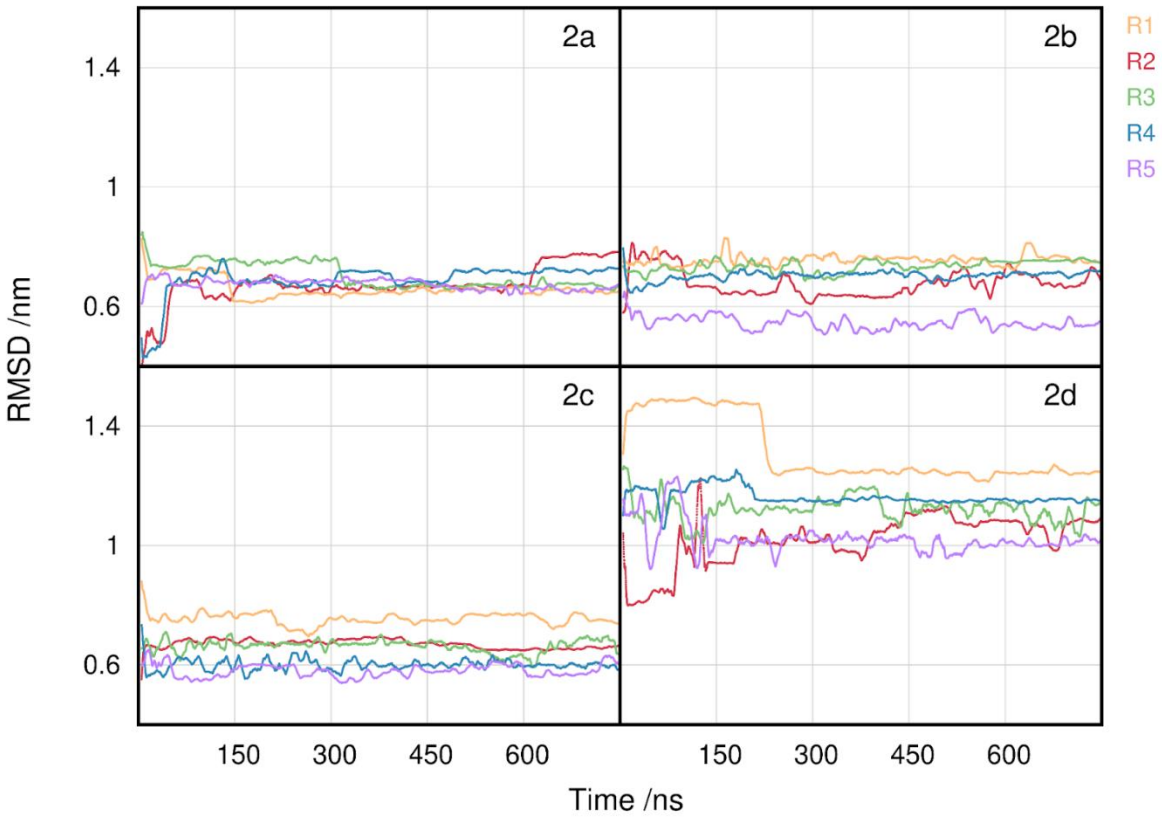

Figure S4. Root mean square deviation (RMSD) of the complex k-RAS + ligand, throughout the simulation time for each replicate simulation.

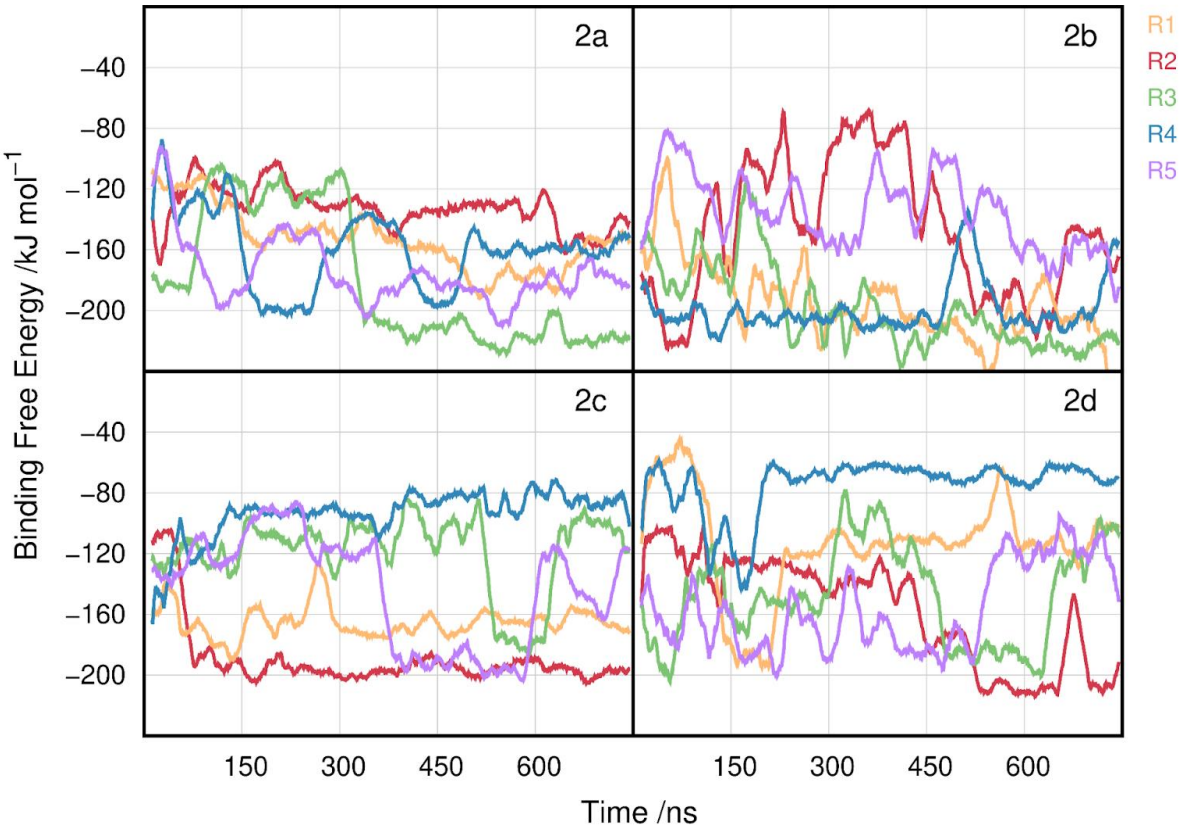

Figure S5. Variation of the MM/PBSA binding free energy between the different ligands and k-RAS for each replicate simulation.

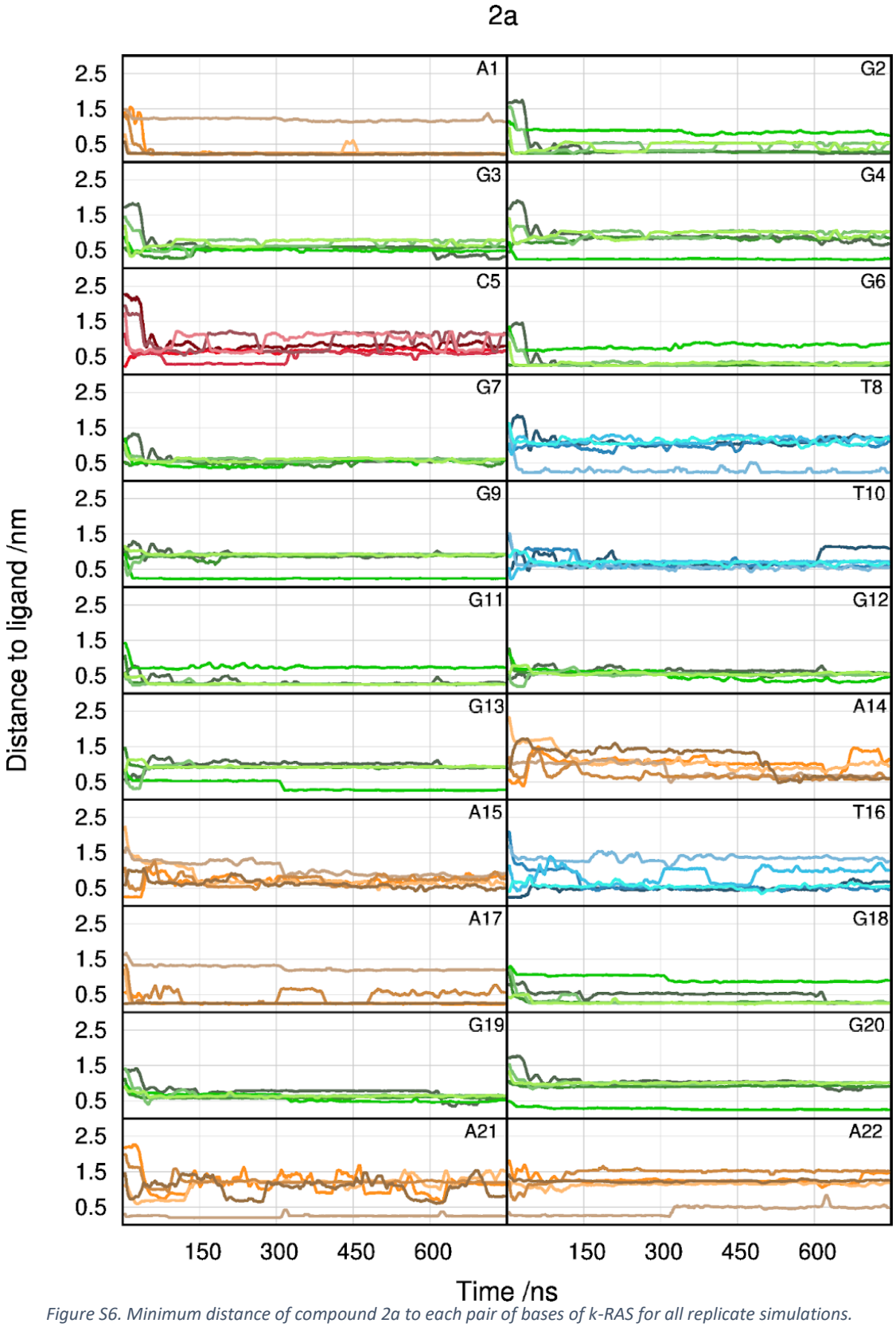

Figure S6. Minimum distance of compound 2a to each pair of bases of k-RAS for all replicate simulations.

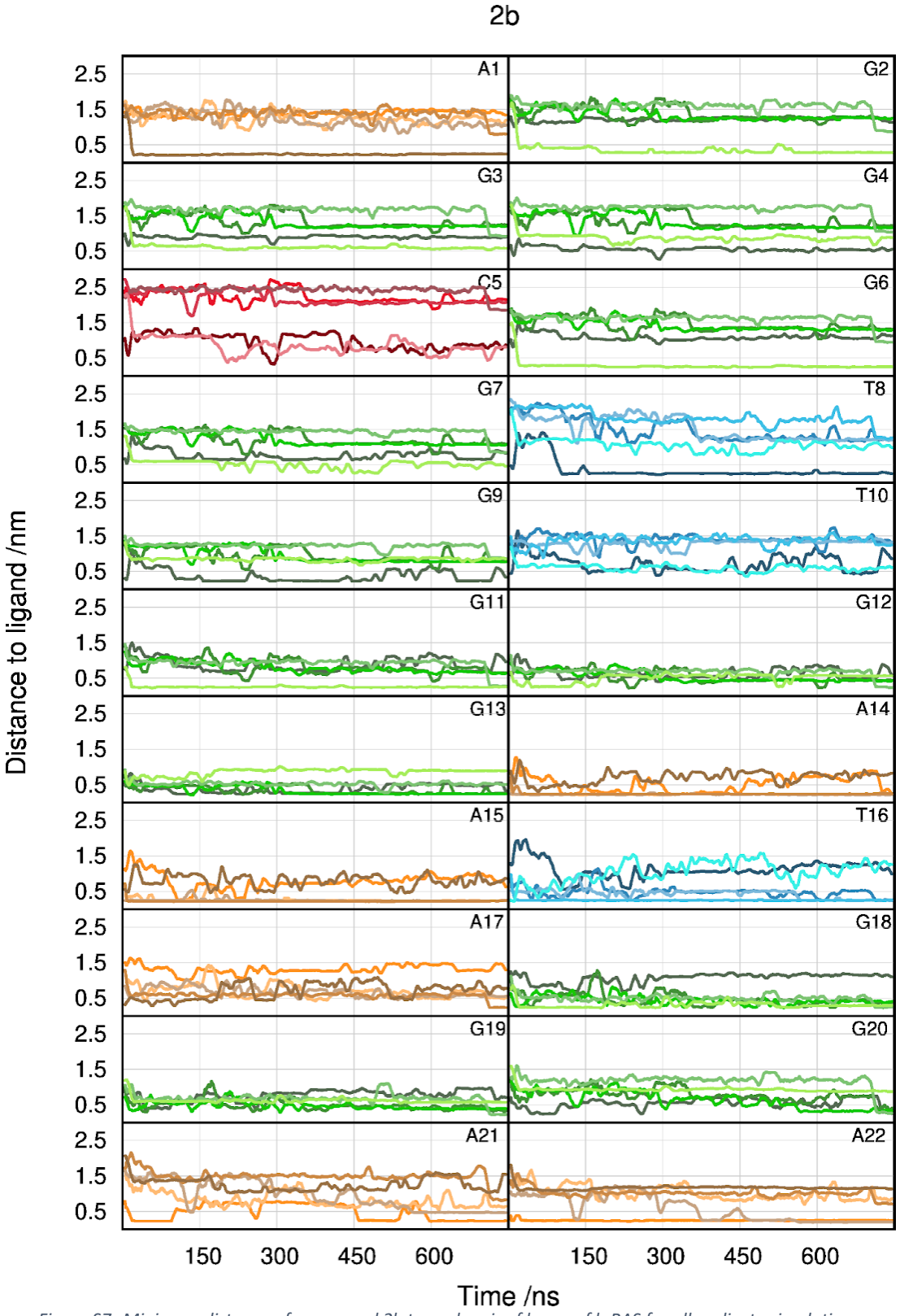

Figure S7. Minimum distance of compound 2b to each pair of bases of k-RAS for all replicate simulations.

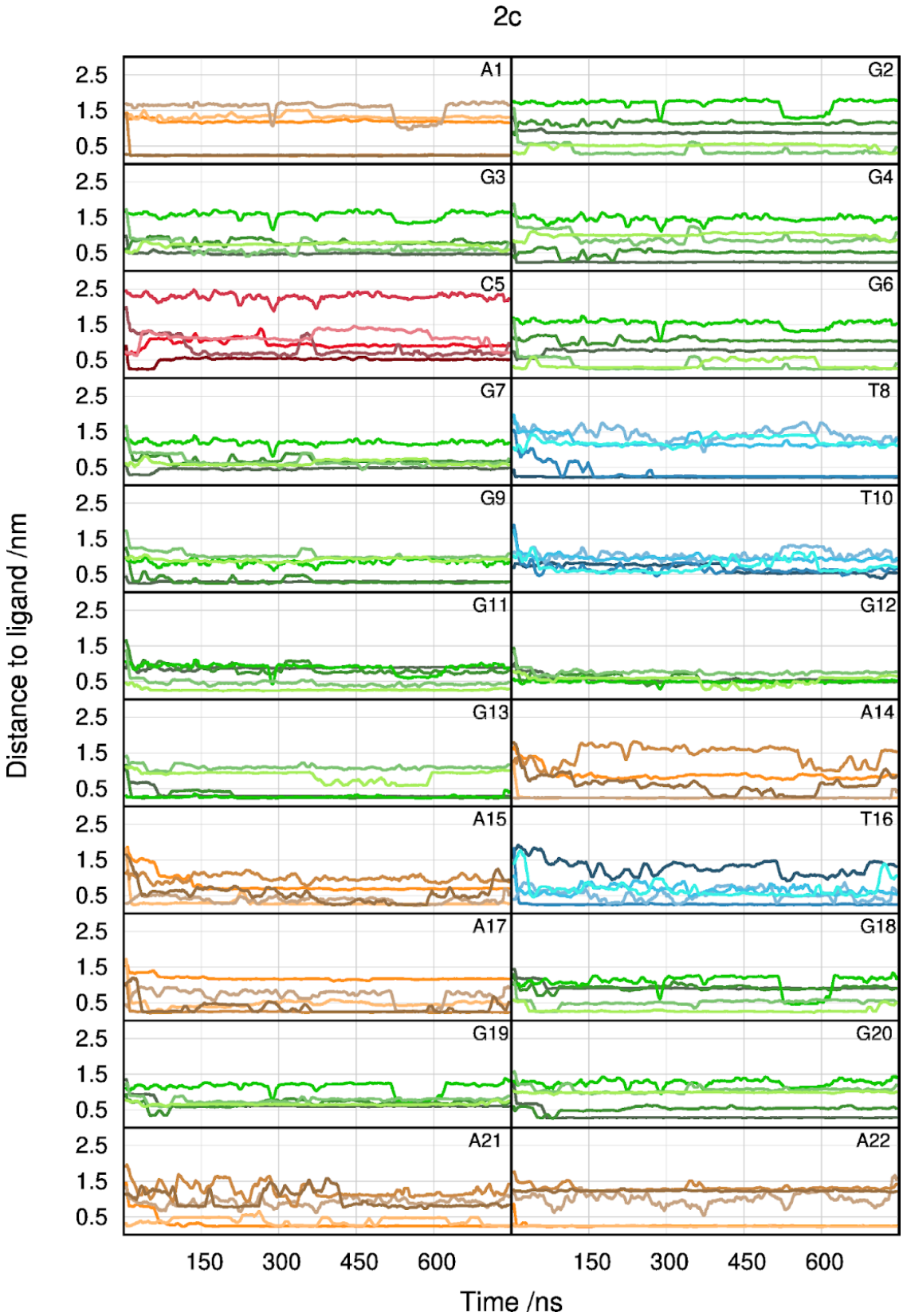

Figure S8. Minimum distance of compound 2c to each pair of bases of k-RAS for all replicate simulations.

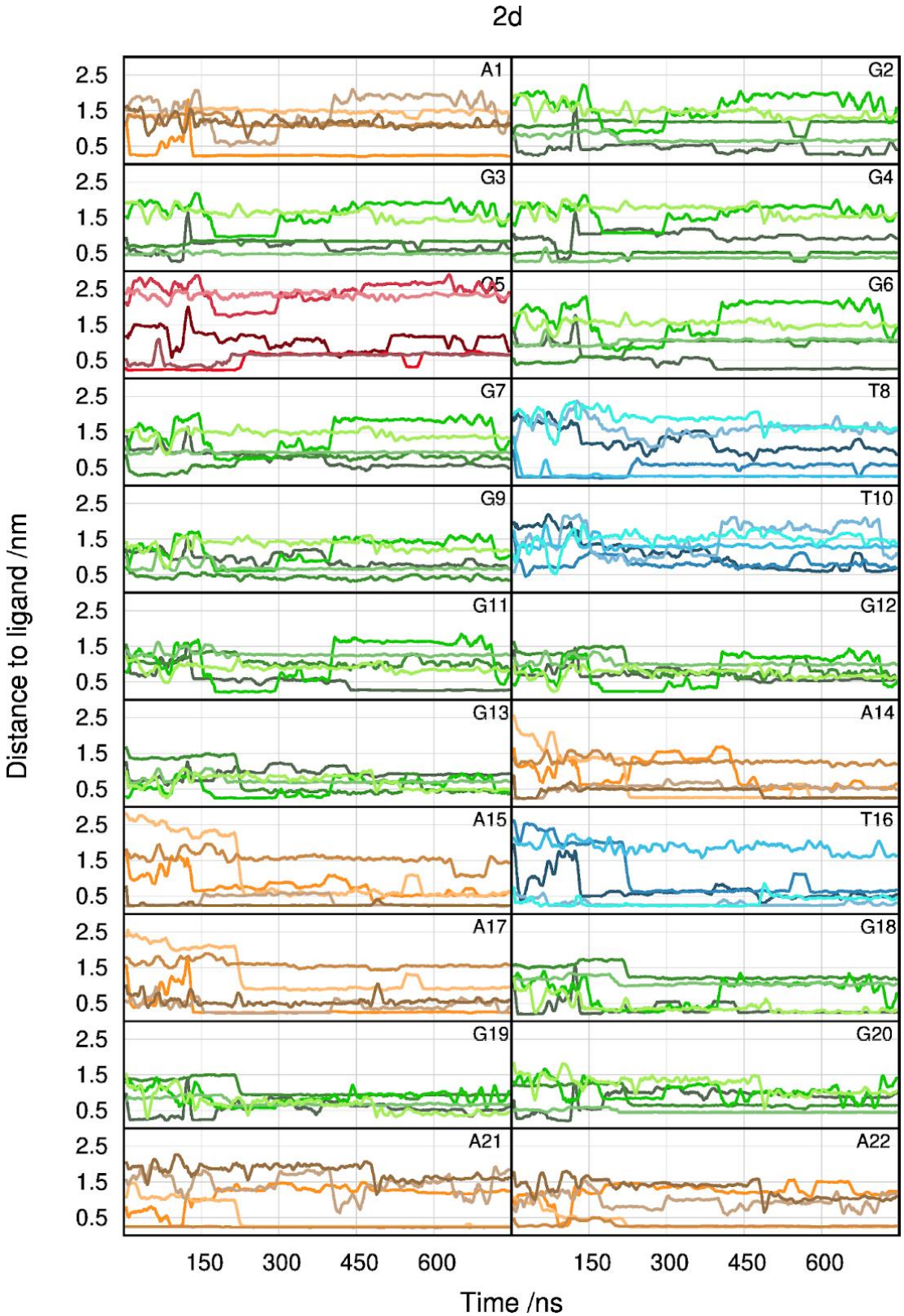

Figure S9. Minimum distance of compound 2d to each pair of bases of k-RAS for all replicate simulations.

NMR spectra

NMR-Spectra were recorded on a Bruker 300 Ultrashield 300MHz, using 300MHz scan for 1H-NMR spectra and 75 MHz for 13C.

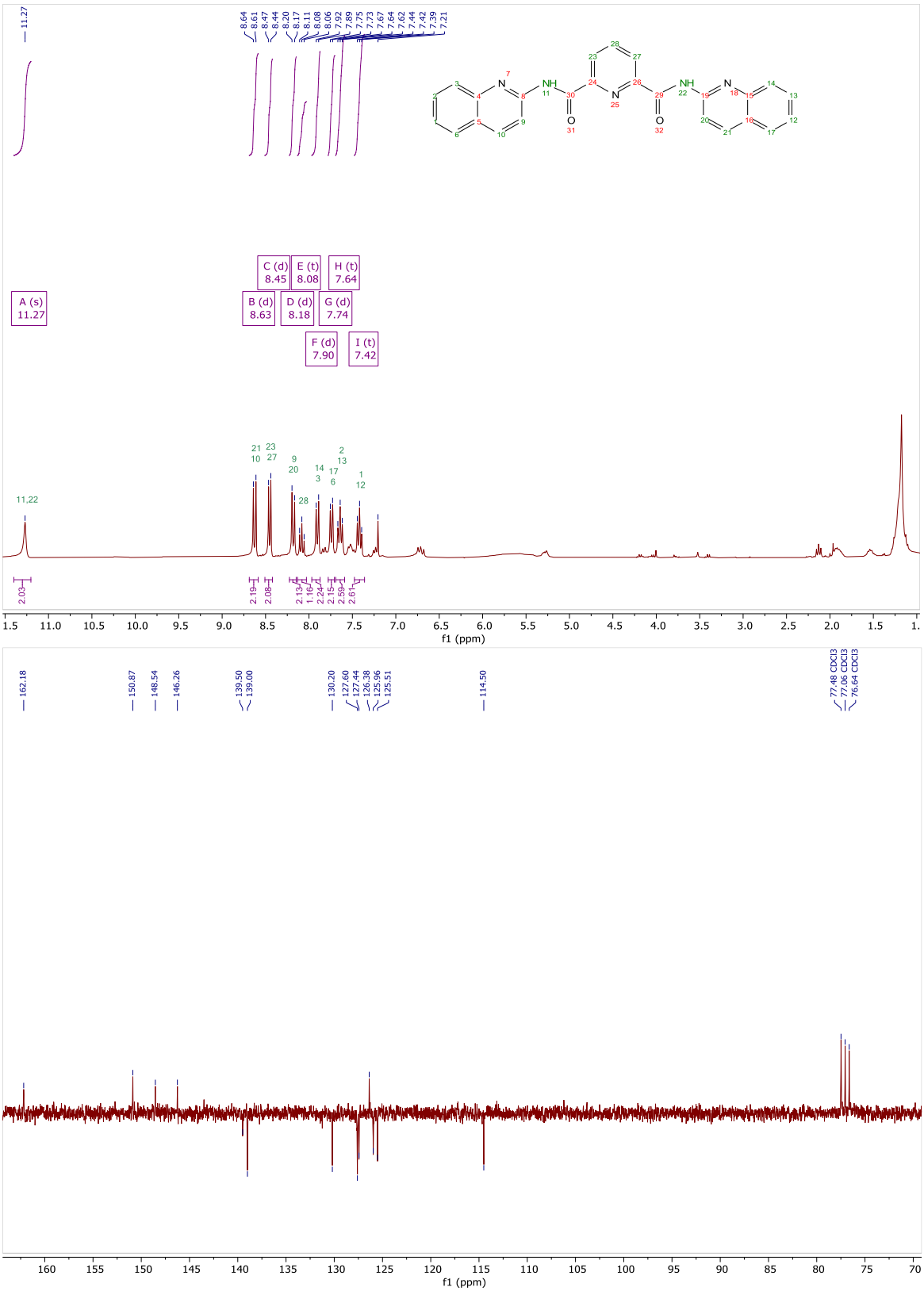

*Figure S10. H-NMR (top) and C-NMR (bottom) spectra of compound **1a**.*

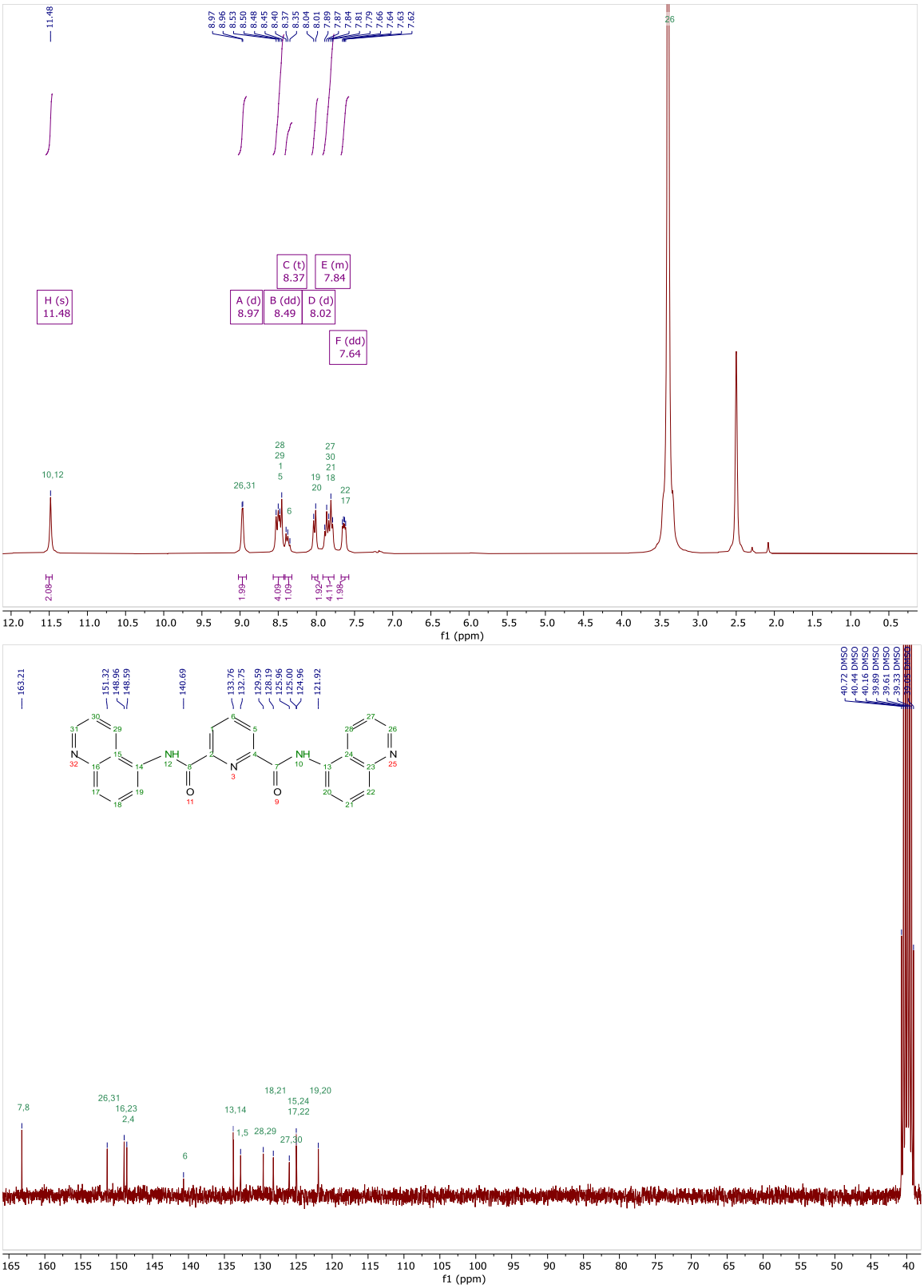

*Figure S11. H-NMR (top) and C-NMR (bottom) spectra of compound **1b.***

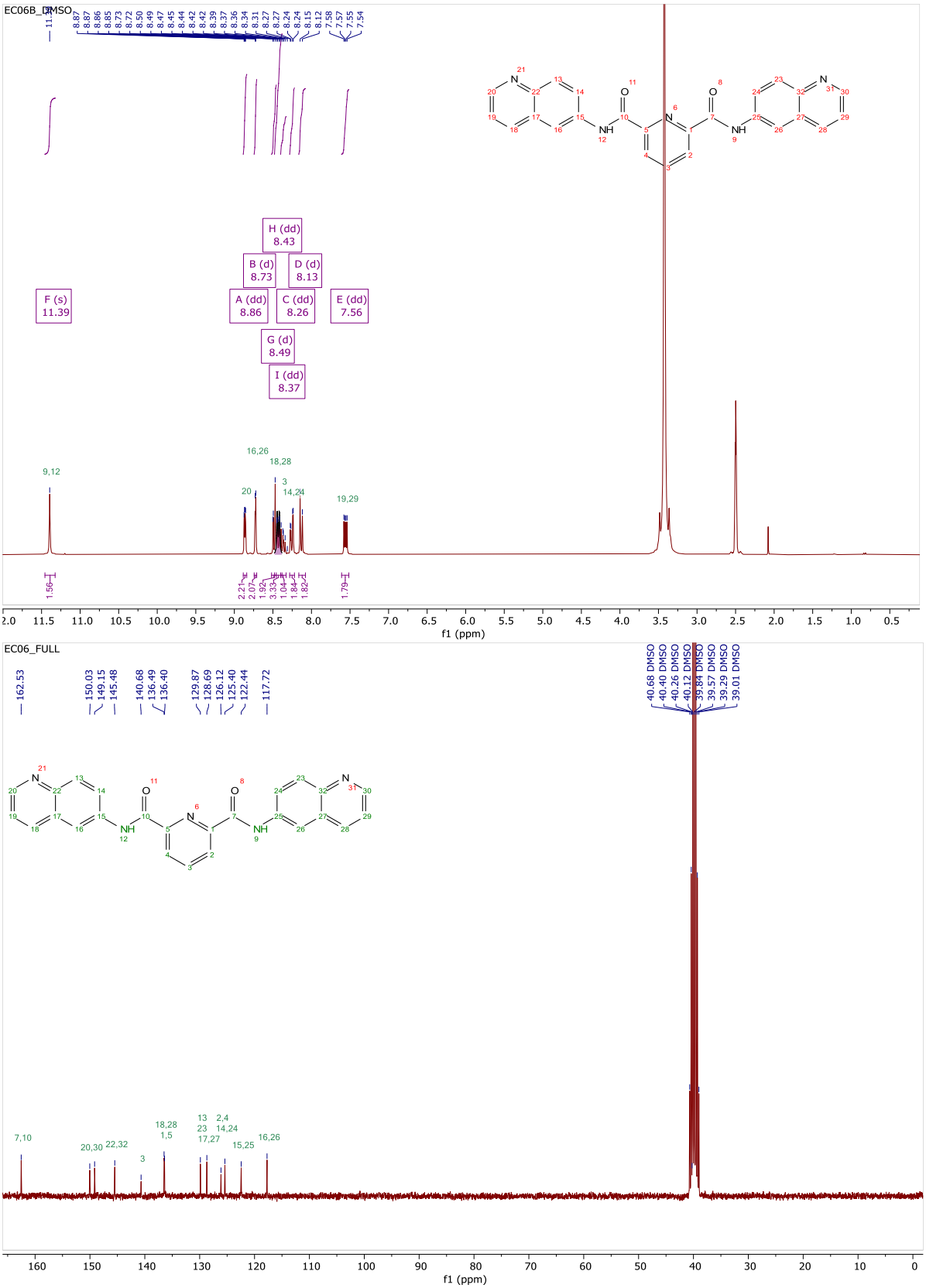

*Figure S12. H-NMR (top) and C-NMR (bottom) spectra of compound **1d.***

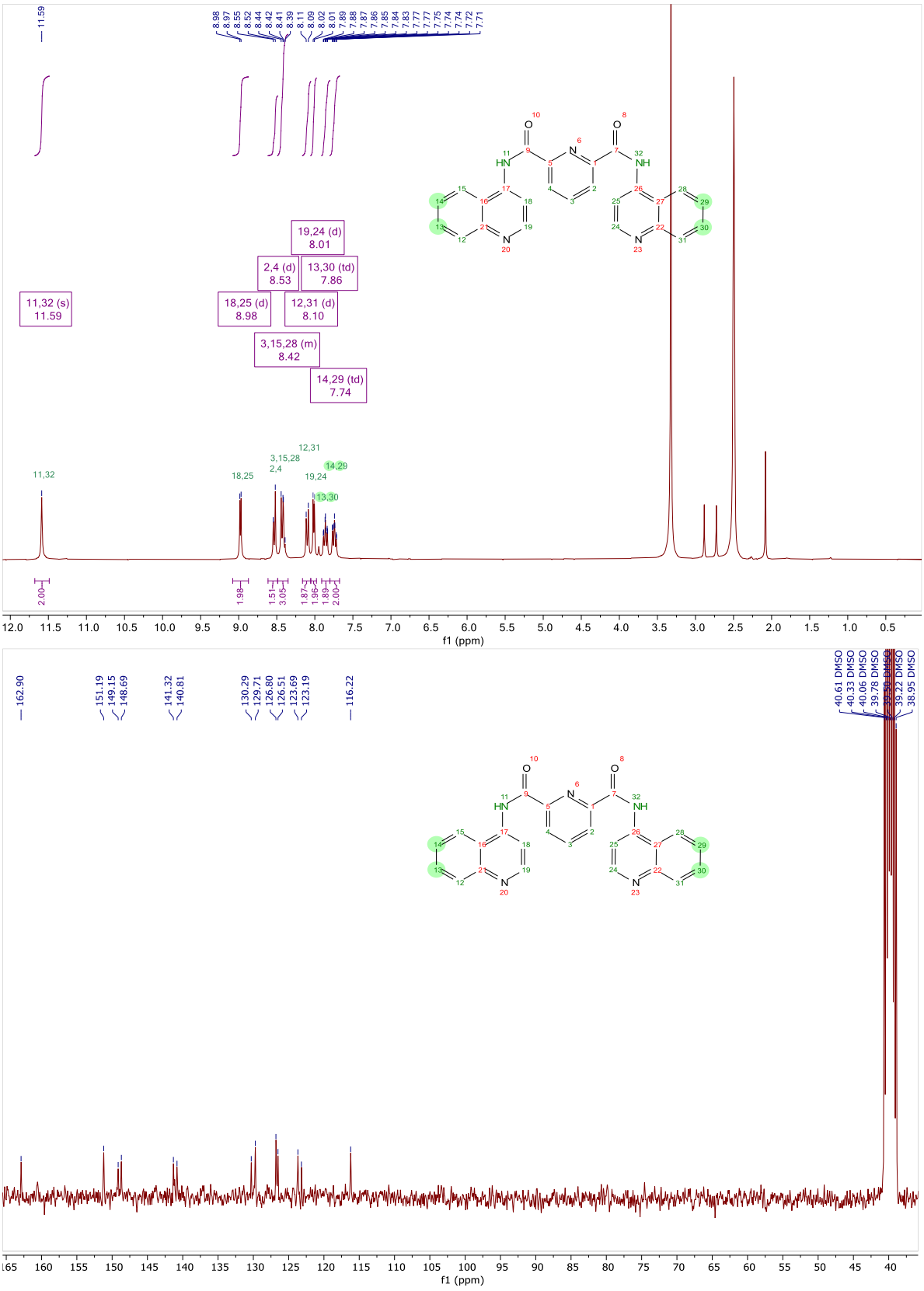

*Figure S13. H-NMR (top) and C-NMR (bottom) spectra of compound **1e**.*

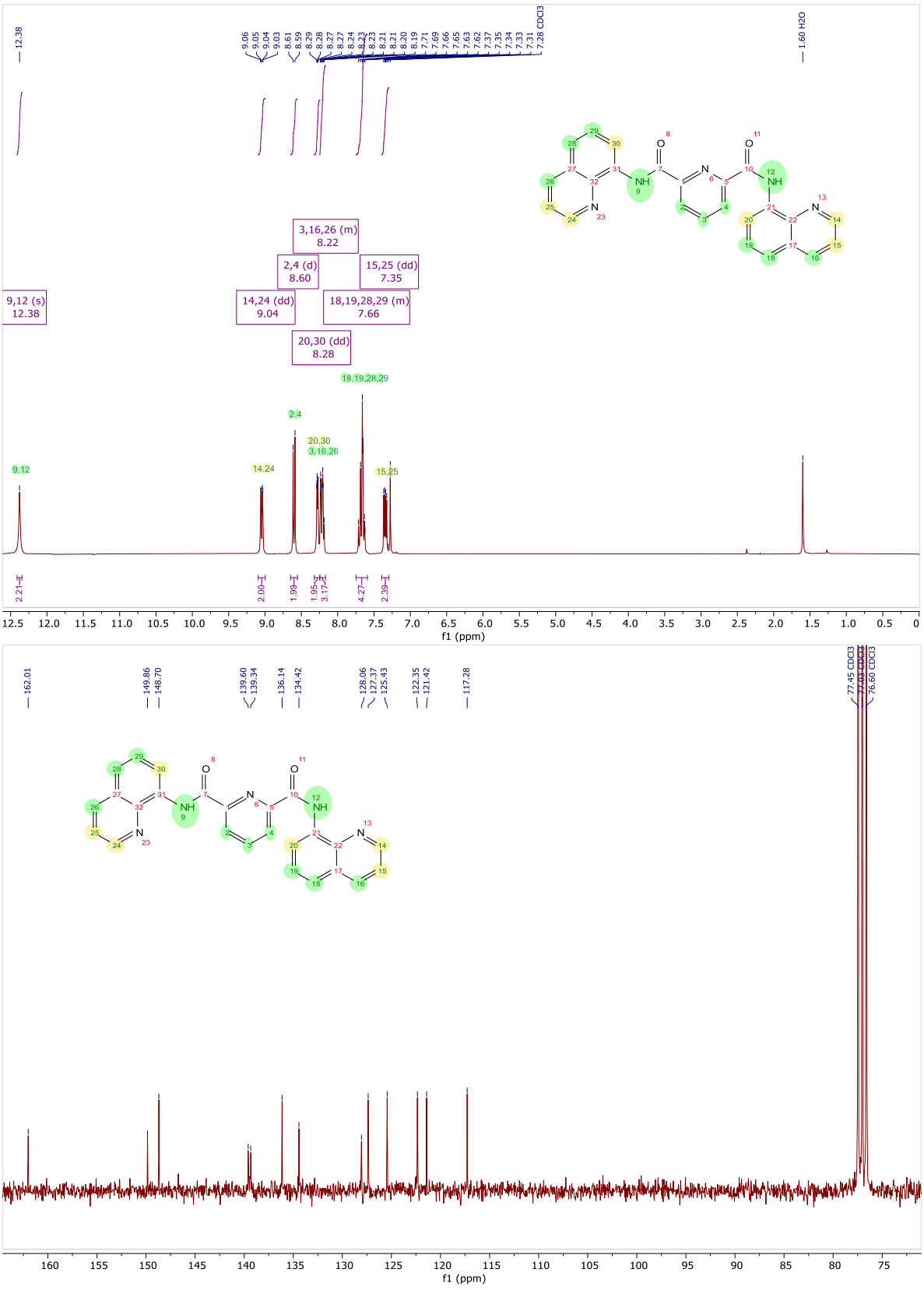

*Figure S14. H-NMR (top) and C-NMR (bottom) spectra of compound **1f.***

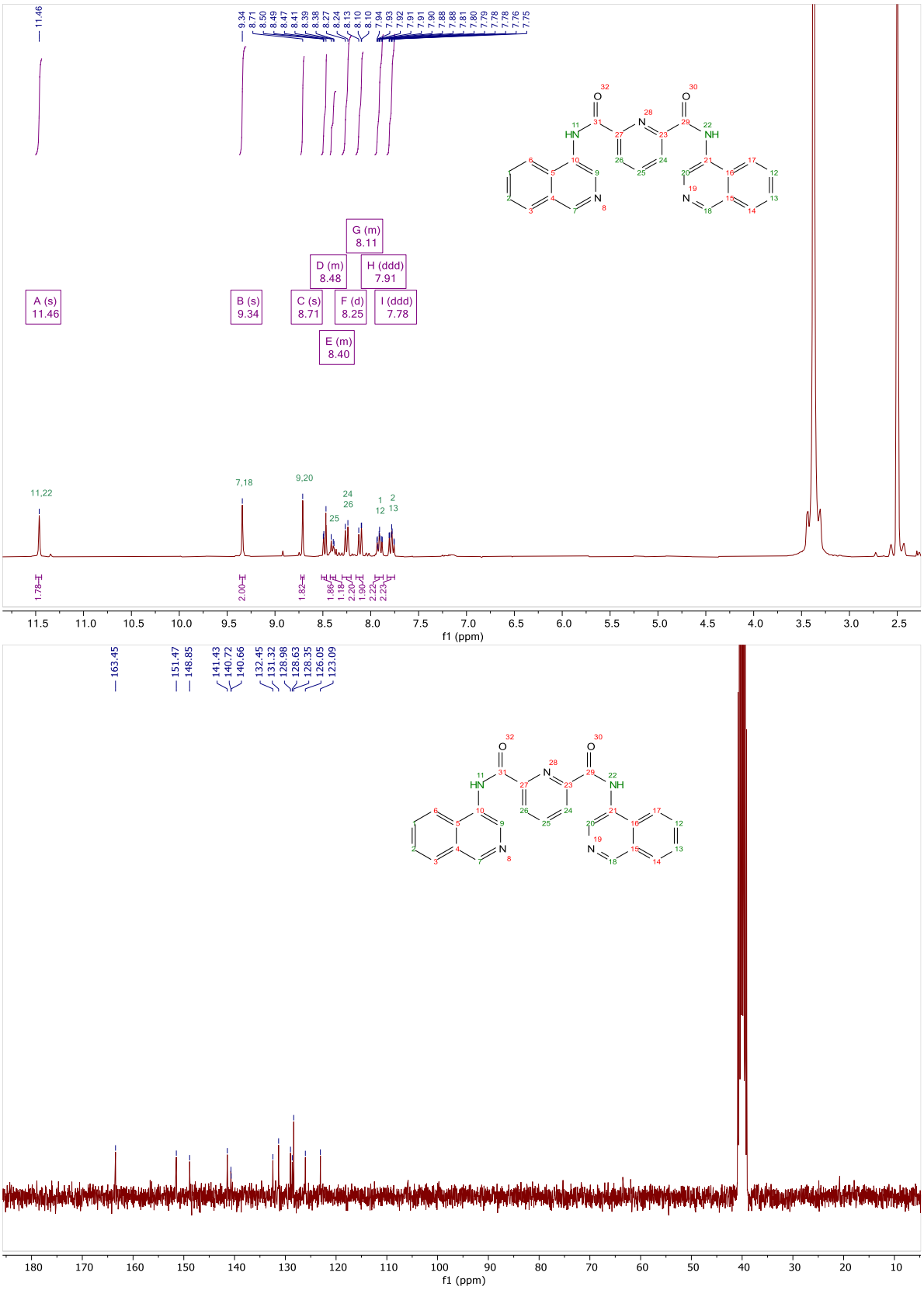

*Figure S15. H-NMR (top) and C-NMR (bottom) spectra of compound **1g**.*

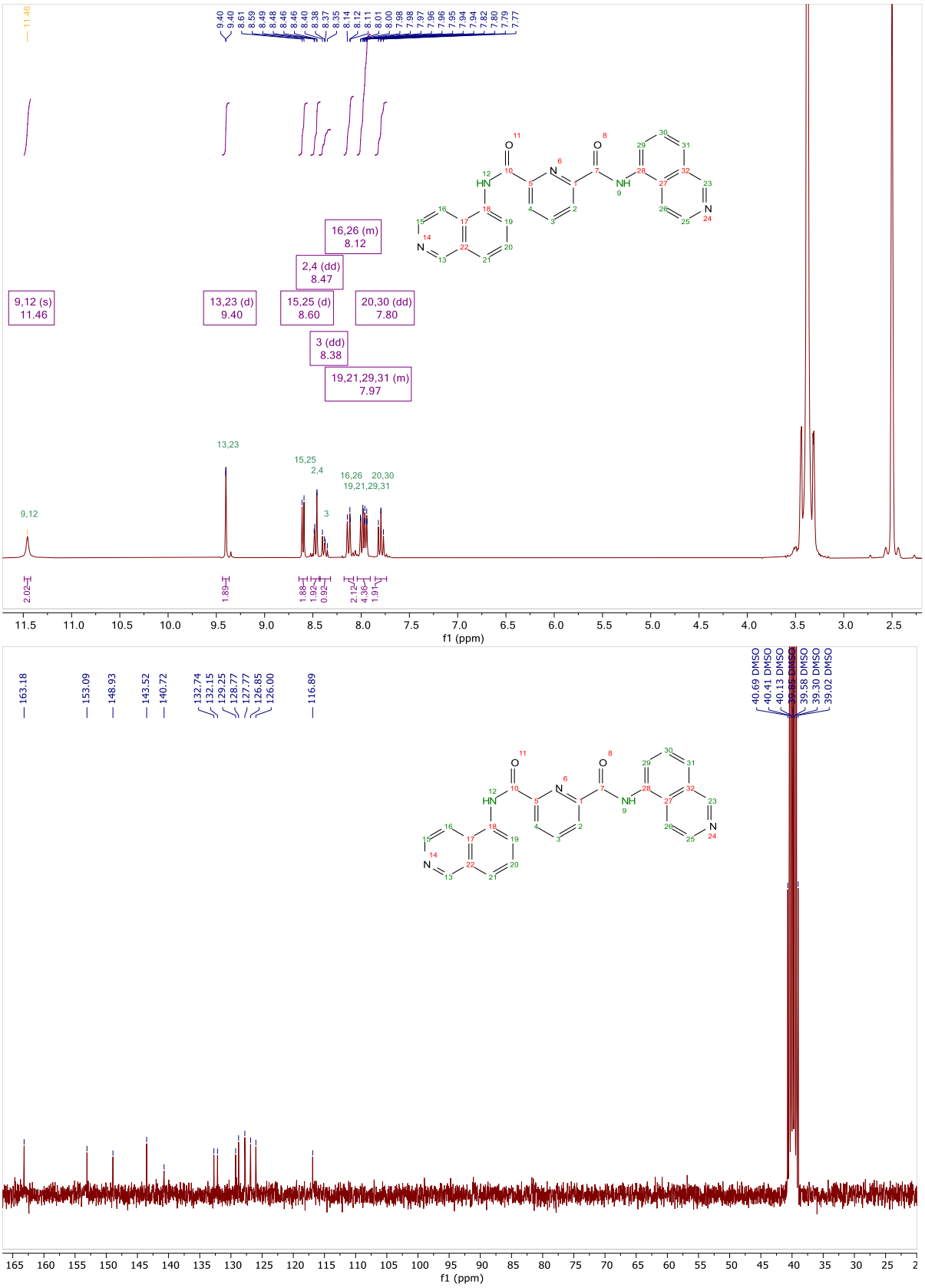

*Figure S16. H-NMR (top) and C-NMR (bottom) spectra of compound **1h.***

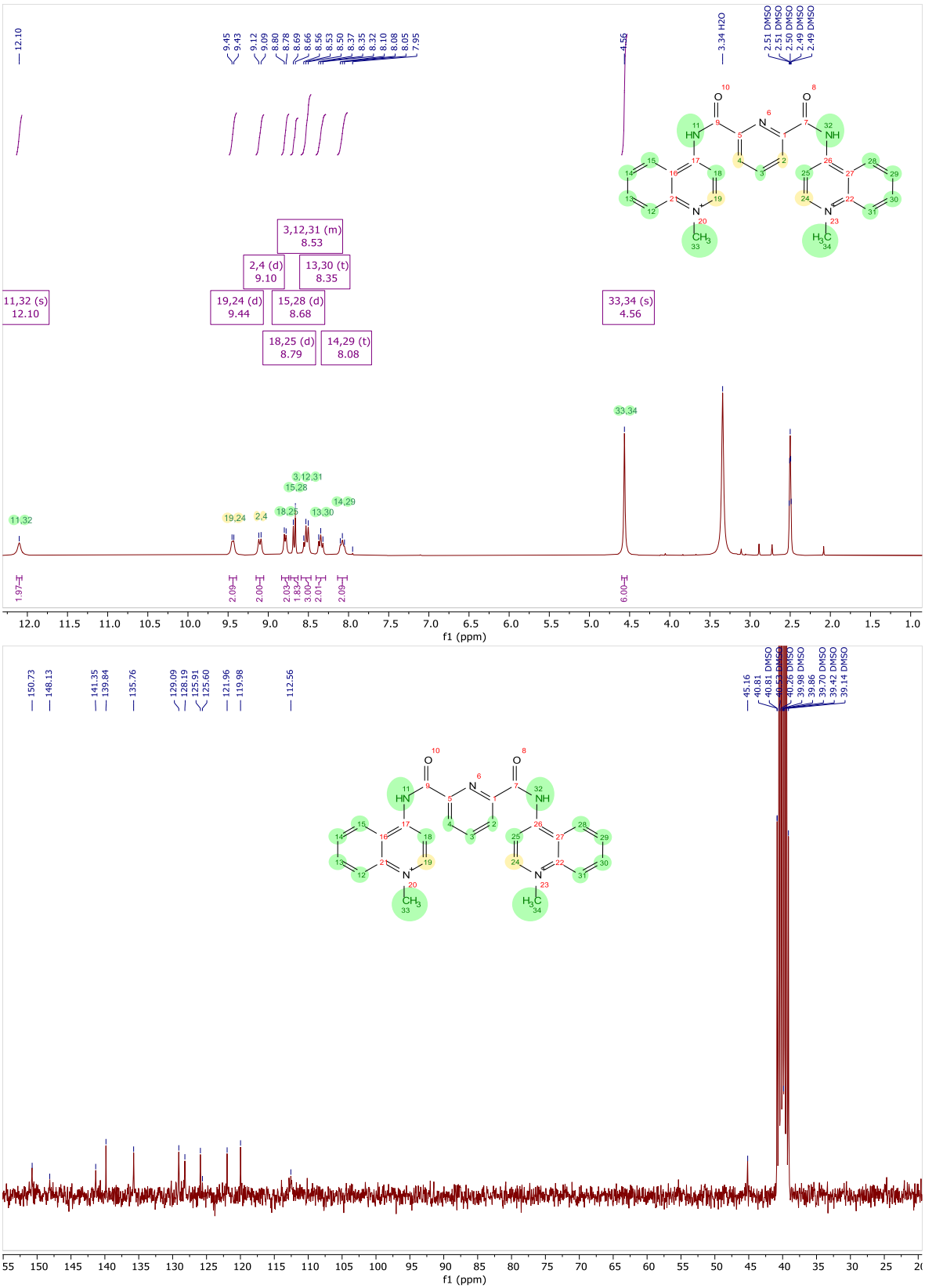

Figure S17. H-NMR (top) and C-NMR (bottom) spectra of compound ***2b.***

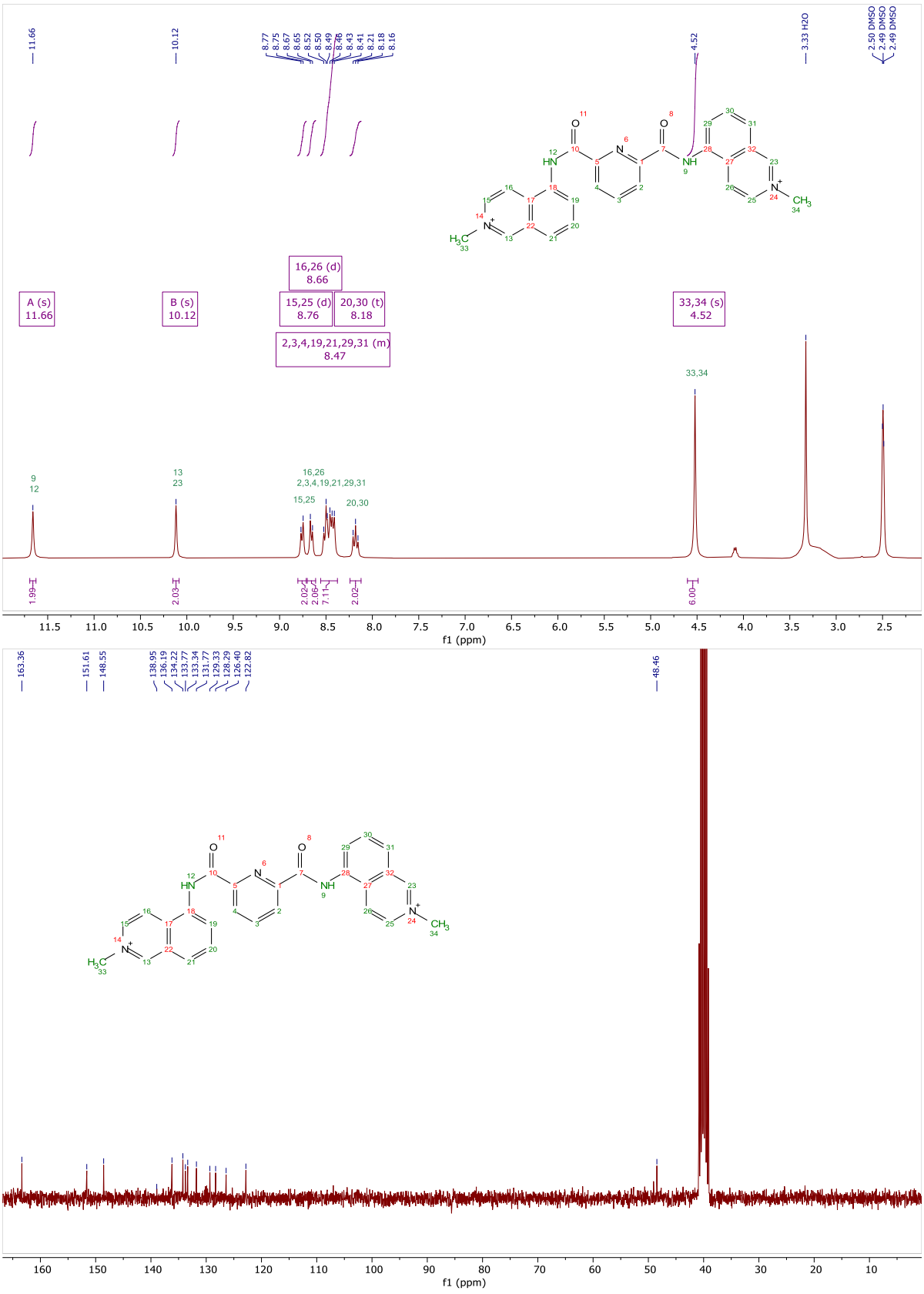

*Figure S18. H-NMR (top) and C-NMR (bottom) spectra of compound **2c.***

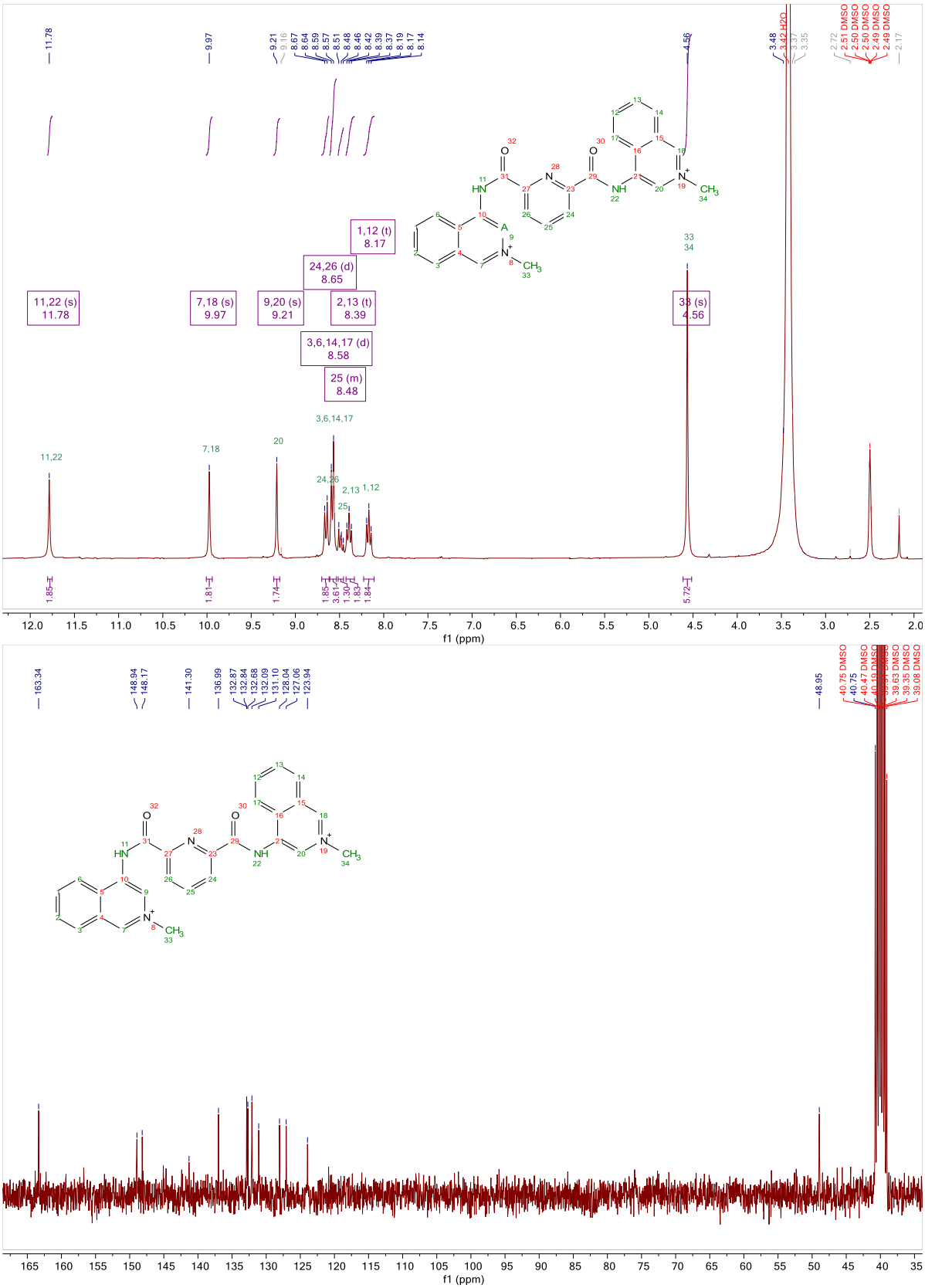

*Figure S19. H-NMR (top) and C-NMR (bottom) spectra of compound **2d**.*

6. Supplemental references

1. Mendes, E.; Cadoni, E.; Carneiro, F.; Afonso, M.B.; Brito, H.; Lavrado, J.; dos Santos, D.J.V.A.; Vítor, J.B.; Neidle, S.; Rodrigues, C.M.P.; et al. Combining 1,3-ditriazolyl-benzene and quinoline to discover a new G-quadruplex interactive small molecule active against cancer stem-like cells. *ChemMedChem* **2019**, cmdc.201900243, doi:10.1002/cmdc.201900243.

2. Hou, T.; Wang, J.; Li, Y.; Wang, W. Assessing the Performance of the MM/PBSA and MM/GBSA Methods. 1. The Accuracy of Binding Free Energy Calculations Based on Molecular Dynamics Simulations. *J. Chem. Inf. Model.* **2011**, *51*, 69–82, doi:10.1021/ci100275a.

3. Bondi, A. van der Waals Volumes and Radii. *J. Phys. Chem.* **1964**, *68*, 441–451, doi:10.1021/j100785a001.

4. Sitkoff, D.; Sharp, K.A.; Honig, B. Accurate Calculation of Hydration Free Energies Using Macroscopic Solvent Models. *J. Phys. Chem.* **1994**, *98*, 1978–1988, doi:10.1021/j100058a043.